Exact modeling of finite temperature and quantum delocalization effects on reliability of quantum-dot cellular automata

2016 J. Phys. D: Appl. Phys. 49 065103

(http://iopscience.iop.org/0022-3727/49/6/065103)

IOP Publishing Journal of Physics D: Applied Physics
J. Phys. D: Appl. Phys. **49** (2016) 065103 (7pp) doi:10.1088/0022-3727/49/6/065103

Exact modeling of finite temperature and quantum delocalization effects on reliability of quantum-dot cellular automata

Juha Tiihonen[1], **Andreas Schramm**[2], **Ilkka Kylänpää**[1] **and Tapio T Rantala**[1]

[1] Department of Physics, Tampere University of Technology, 33720 Tampere, Finland
[2] Optoelectronic Research Centre, Tampere University of Technology, FI-33101 Tampere, Finland

E-mail: juha.tiihonen@tut.fi

Received 2 November 2015, revised 9 December 2015
Accepted for publication 16 December 2015
Published 11 January 2016

Abstract

A thorough simulation study is carried out on thermal and quantum delocalization effects on the feasibility of a quantum-dot cellular automata (QCA) cell. The occupation correlation of two electrons is modeled with a simple four-site array of harmonic quantum dots (QD). QD sizes range from 20 nm to 40 nm with site separations from 20 nm to 100 nm, relevant for state-of-the-art GaAs/InAs semiconductor technology. The choice of parameters introduces QD overlap, which is only simulated properly with exact treatment of strong Coulombic correlation and thermal equilibrium quantum statistics. These are taken into account with path integral Monte Carlo approach. Thus, we demonstrate novel joint effects of quantum delocalization and decoherence in QCA, but also highly sophisticated quantitative evidence supporting the traditional relations in pragmatic QCA design. Moreover, we show the effects of dimensionality and spin state, and point out the parameter space conditions, where the 'classical' treatment becomes invalid.

Keywords: quantum-dot cellular automata, path integral Monte Carlo, quantum delocalization

(Some figures may appear in colour only in the online journal)

I. Introduction

Quantum-dot cellular automata (QCA) is a paradigm for nanoscale logic circuitry [1], which has been studied extensively during the past two decades. It is a promising candidate for replacing the current complementary metal-oxide-semiconductor (CMOS) computing technology. The problem with CMOS is that it is reaching its fundamental size limitations: the heat generation and quantum effects interfere with the desired operation at extremely small scales. Conversely, QCA devices present the possibility to address both of these concerns by minimizing power dissipation and using the 'undesirable' quantum effects to actually perform its calculations. Since its discovery, QCA has inspired a huge number of proposed structures [2–7] and experimental realizations [8–11].

While QCA is based on localization of single electrons inside cellular quantum dot (QD) structures, it is critically sensitive for such conditions as finite temperature, particle density, geometry and fabricational imperfections [12–14]. Thus, the operability and fabrication of QCA are subject to several fundamental restrictions, the most significant of which is the temperature. It is related to the geometrical scale of the device, so that room temperature operation is only expected from molecular [15–17] and magnetic [18] QCA concepts with $\sim$1 nm features. Metal plate [19, 20] and semiconductor [10] techniques with $\sim$10–100 nm features have also been demonstrated, but only at cryogenic temperatures.

The development of QCA gains a lot from the hierarchy of computational simulation models. However such bistable and strongly correlated system is challenging to approach with iterative and mean-field approaches that are often used in electronic structure calculation. Thus, the most widely used models are the extended Hubbard model and Hartree approximation [21] and nonlinear two-state model, employed in the popular QCADesigner simulation tool [22]. However, accessing nonideal properties, such as tolerance

of fabricational imperfections, missing electrons, dot displacement or finite temperature, calls for more sophisticated methods [6, 13, 15, 16, 23–25]. This kind of analysis and pursuit of more robust and more complicated QCA designs is an important step towards experimental feasibility [4, 26].

The focus of this work is not on the QCA paradigm, but rather on the fundamental thermal physics beyond quantum limit of the QCA building blocks, the four-site cell structures. This involves pushing the limits of modeling sophistication by employing path integral Monte Carlo (PIMC) method [27]. PIMC has inherent account of finite temperature equilibrium and charge carrier correlation, and hence, it is most suitable tool to approach such strongly correlated QD systems [28–30]. By introducing QD overlap in our model parameters, we become the first to simulate high electronic delocalization in QCA. While this is not, pragmatically, the desired region for operation, the transition from trivial trends into novel quantum statistical phenomena is insightful, to say the least. Also, the methods established here could prove useful in the quantum physical aspects of QCA, such as exchange frequencies, adiabatic switching and the 'null' state [21].

II. Model and methods

A single QCA cell consists of two excess electrons in a lateral array with four sites (or QDs), as shown schematically in figure 1. We model it with an external potential defined by

$$V_{\mathrm{QCA}} = \min_i \left[V_i(\boldsymbol{r})\right], \tag{1}$$

where the harmonic (or parabolic) potential of each site centered at $\boldsymbol{r}_i$ is

$$V_i(\boldsymbol{r}) = \frac{1}{2} m^* [\boldsymbol{\omega} \cdot (\boldsymbol{r} - \boldsymbol{r}_i)]^2, \tag{2}$$

where m^* is the effective mass of electrons and $\boldsymbol{\omega} = (\omega_x, \omega_y, \omega_z)$ is the confinement strength. The side of the QCA square (lattice constant) a varies between 20 nm … 100 nm. Most of this range is within the scope of current state-of-the-art semiconductor quantum dot technology [31]. Indeed, the medium properties are chosen according to those of GaAs/InAs quantum dots (in 300 K [32]): effective mass is $m^* = 0.063\, m_{\mathrm{e}}$, where m_{e} is the free electron mass, and (static) dielectric constant $\varepsilon = 12.9$ is used to scale the exact $1/r$ Coulomb repulsion of electron–electron interaction.

The 'size' L of a single QD is estimated by comparing the 'effective confinement' induced by ω to that of a simple quantum well, where the concept size is obvious. By setting the ground state energies of these two equal in one dimensional case, it is easy to see that it leads to condition

$$\omega = \frac{\pi^2 \hbar}{L^2 m^*}. \tag{3}$$

Alternatively, by using least squares fitting to minimize the difference between the ground state charge densities the same relation is found, but π is replaced with approx. 3.50. Thus, it is fair to notice that the concept of QD size is not free of ambiguity. The confinements used in this work are obtained from equation (3) and presented in table 1. The potential barrier between adjacent sites varies between approximatively 2 meV–57 meV with $L = 40$ nm and 36 meV–920 meV with $L = 20$ nm.

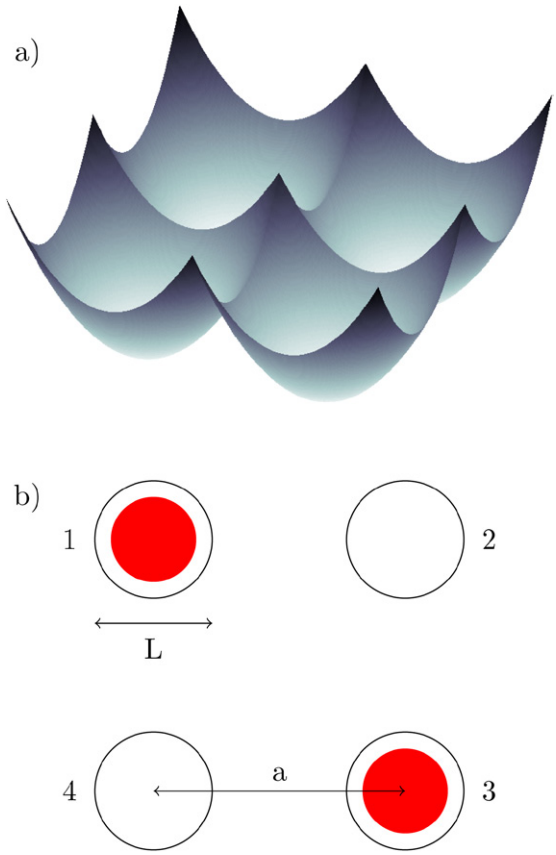

Figure 1. (a) A visualization of harmonic confinement potential of our QCA cell model. (b) Schematic picture of an ideal QCA setup, where the two electrons occupy either '0' bit (sites 1 and 3) or '1' bit (sites 2 and 4). The site separation a and QD size L are marked.

An ideal four-site QCA system is bistable, i.e. in the ground state the two electrons may occupy either one of the two possible combinations of opposite sites: sites 1 and 3, or 2 and 4 in figure 1. The polarization of the state is defined [1] as

$$P = \frac{p_1 - p_2 + p_3 - p_4}{p_1 + p_2 + p_3 + p_4}, \tag{4}$$

where p_1 is the electron occupation density at site 1, and so on. Here, the site boundaries (for occupation density) are those of the four quadrants about the center of the cell. By convention, polarization $P = 1$ is labeled the '0' bit and $P = -1$ the '1' bit [1]. Deviation from these extreme values implies reduction in reliability, and vice versa.

Without external 'driver bit', the average polarization of single cell in thermal equilibrium is zero due to symmetry. Hence, we introduce *fidelity* to describe the occupation correlation of two electrons localized in the four-site system:

$$F = \begin{cases} 1 & \text{at opposite sites} \\ 0 & \text{at adjacent sites} \\ -1 & \text{at the same site.} \end{cases} \tag{5}$$

An equivalent formulation in terms of polarization is

Table 1. QD sizes L and corresponding confinements strengths ω.

L (nm)	L (a.u.)	ω (a.u.)
40 nm	756	0.000 274
30 nm	567	0.000 487
20 nm	378	0.001 10
10 nm	189	0.004 38
5 nm	94.5	0.0175

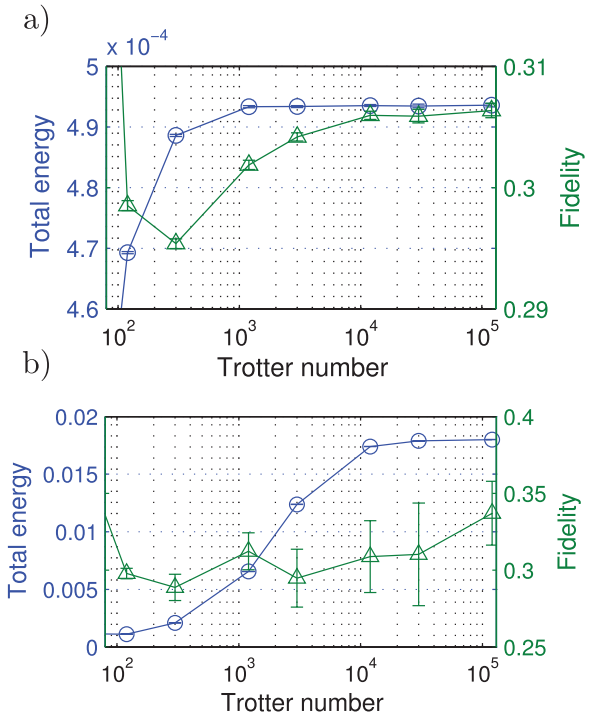

Figure 2. Convergence of total energy (blue circles) and fidelity (green triangles) as functions of Trotter number at $T = 0.85$ K using 2D (a) and 3D (b) models with $L = 40$ nm at $a = 20$ nm separation.

$$F = |P| - 2\delta, \tag{6}$$

where δ is an overlap term, i.e. $\delta = 1$ if the two electrons occupy same site, and otherwise $\delta = 0$. The bistable ground states give $\langle F \rangle \to 1$, whereas completely uncorrelated distribution leads to $\langle F \rangle \to 0$. In the hypothetical case of attractive interaction, the electrons would tend to occupy the same sites, hence $\langle F \rangle \to -1$.

Of course, in finite temperature, the average fidelity is between 0 and 1. This is described by the density matrix, which corresponds to wave function in zero Kelvin. Our approach is to simulate thermal equilibrium in a fixed temperature and evaluate the density matrix and partition function for interacting electrons using Feynman path-integral approach to quantum statistical physics [33]. The partition function is given as the trace of the density matrix

$$Z = \mathrm{Tr}\ \hat{\rho}(\beta) = \int \mathrm{dR}_0 \mathrm{dR}_1 \ldots \mathrm{dR}_{M-1} \prod_{i=0}^{M-1} \mathrm{e}^{-S(R_i, R_{i+1}; \tau)}, \tag{7}$$

where $\hat{\rho}(\beta) = \mathrm{e}^{-\beta \hat{H}}$, S is the action, $\beta = 1/k_B T$, $\tau = \beta/M$, $R_M = R_0$ and M is called the Trotter number. The simulation with singular electron–electron interaction is exact for the electronic correlations, but of course, within the numerical accuracy, which is given by the imaginary-time 'time-step' $\tau = 1\,(\mathrm{au})^{-1} \approx 24 \times 10^{-18}$ s.

The partition function description in equation (7) only holds for distinguishable particles as such. Thus, in two electron system, we assume opposite spins (singlet state; one spin-up and one spin-down) and treat the electrons as 'boltzmannons', i.e. they obey the Boltzmann statistics. Usually, the triplet state contribution is considered negligible due to the low electronic interaction [1]. However, in case of highly nonlocalized electron densities (weak confinement) the account of exchange interaction may become significant, especially when invoked with external magnetic control. Hence, we also consider the effects of the triplet state by using restricted path-integral Monte Carlo (RPIMC) with free-particle nodes [34, 35].

Using Metropolis procedure [36] with bisection sampling [37] extended with an efficient displacement scheme, we obtain the exact thermal equilibrium quantum statistics. That is, the ensemble of all possible quantum paths of the two interacting electrons in the four-site system are sampled with the correct distribution. The numerical subtleties and details about PIMC can be found elsewhere [27, 38].

III. Results

The accuracy of PIMC description depends on imaginary time step τ. Hence, we start with a convergence consideration for finding the appropriate values for simulation parameters. According to equation (7), this basically means finding the Trotter number M large enough to properly describe the 'quantum nature' of particles in each individual case. Curiously, the special case $M = 1$ is considered the 'classical' limit, and will also be investigated as a reference.

To find the limiting time step τ, we consider the values of both total energy and fidelity as functions of M in our most challenging case: $a = 20$ nm, $T = 0.85$ K and $L = 40$ nm. This is illustrated in figure 2 in both 2D (a) and 3D (b). Both curves exhibit monotonous convergence in total energy, and a vast drop in fidelity, followed by a slow adjustment to convergence. Due to data fluctuations and error bars, the convergence of fidelity in 3D is not perfectly pronounced, but we end up with $M = 12\,000$, that is $\tau \approx 1$ for two reasons. Firstly, $M = 12\,000$ is computationally feasible and still amply sufficient for any 2D simulation. Secondly, any error in fidelity is only a few percent in magnitude and also strongly localized in parameter space. Indeed, additional convergence calculations indicate no error while proceeding towards less demanding parameters, i.e. $a \geqslant 20$ nm, $T \geqslant 0.85$ K and $L \leqslant 40$ nm. Thus, for consistency, we keep $\tau \approx 1$ in all simulations.

The dominating effect on electronic correlation, i.e. the fidelity from equation (5), is that of the finite temperature. The mechanism of correlation decay is visualized in *correlation density* plots, figure 3. In these plots the density distribution of one electron is plotted according to the reference electron positioned at the bottom-left site of the cell (marked with a circle). In ideal (ground state) case the density distribution is

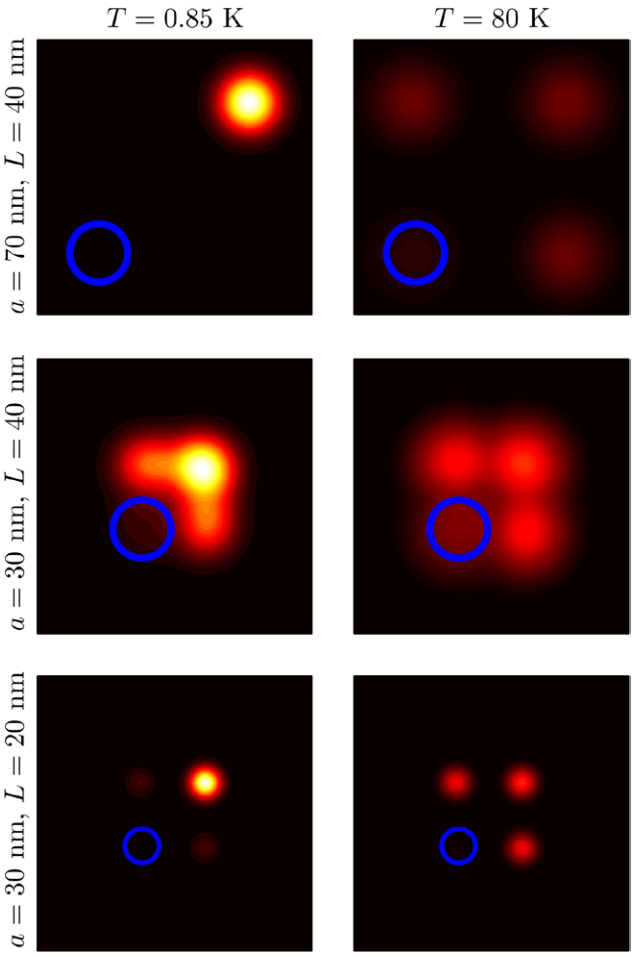

Figure 3. The density distribution of one electron is plotted according to the reference electron (blue circle) at $T = 0.85$ K (left) and $T = 80$ K (right) with different separation distances and QD sizes. The normalization is the same in both temperatures.

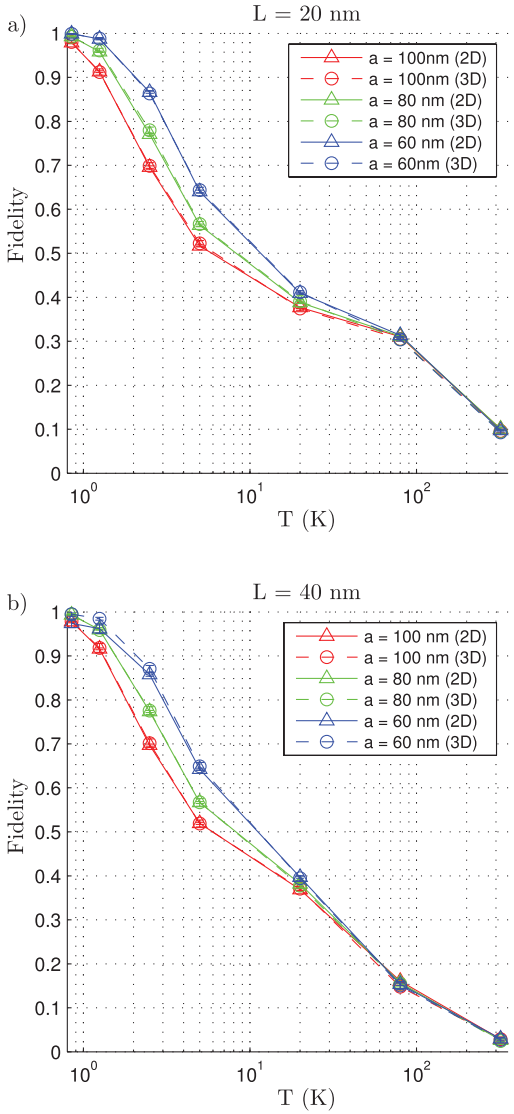

Figure 4. Fidelity with two QD sizes, $L = 20$ nm (a) and $L = 40$ nm (b), is computed at various long QD separations a and temperatures of 0.85 K, 1.25 K, 2.5 K, 5 K, 20 K, 80 K and 320 K. The 3rd dimension is a $L_z = 5$ nm cavity.

localized at the top-right site. High temperature induces delocalization, i.e. leakage of the electronic density to the neighbouring cell sites. At low temperatures and weak confinement, this is also caused by quantum delocalization, which is demonstrated by comparing $L = 20$ nm and $L = 40$ nm QDs at 30 nm separation. Thus, strong confinement is more tolerant to delocalization.

Now, the thermal equilibrium values for fidelity are computed for different lattice constants a, QD sizes L, and temperatures T. The typical QCA picture with strictly localized electronic densities is achieved by using longer separations a (60 nm, 80 nm, 100 nm) for two different QD sizes, $L = 20$ nm and $L = 40$ nm, in figure 4, respectively. Results for both 2D and 3D are shown, the latter of which confines electrons with $L_z = 5$ nm cavity along z-axis. Clearly, we can make the following trivial conclusions: With large separations, fidelity increases with

- decreasing temperature (strongly)
- decreasing QD separation distance a at low temperatures
- decreasing QD size L, i.e. increasing confinement

The effect of dimensionality is negligible.

Next, the same fidelity curves are repeated at shorter cell separations a. This allows for the investigation of conditions and implications of the seldom considered quantum delocalization effects. Figure 5 illustrates how fidelity drops considerably at low temperatures as the QDs are brought sufficiently close to each other. Obviously, the drop is due to the overlap in electron densities, which do not maintain localized single-QD shape anymore. Instead, the particles are delocalized over QD potential barriers while still maintaining some correlation effect. It appears that the delocalization drop in fidelity

- only appears at low temperatures
- is decreased by increasing QD separation distance a at low temperatures
- is increased by increasing QD size, i.e. decreasing confinement

The dimensionality makes a difference so that the 3D model is more localized, but only near the threshold value for a. This is the quantum limit for QCA fidelity, where the

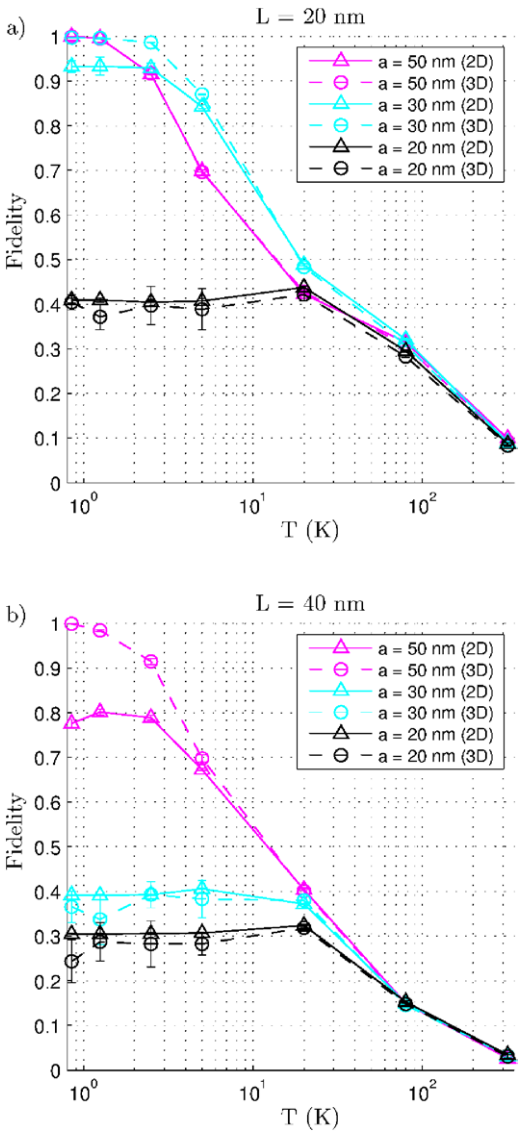

Figure 5. Fidelity results similar to those in figure 4 are repeated with shorter QD separations a. Again, we have $L = 20$ nm (a) and $L = 40$ nm (b).

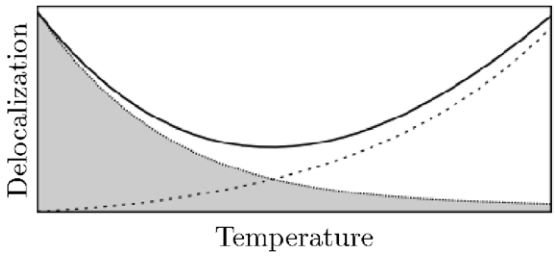

Figure 6. A schematic separation of the total delocalization (solid line) to thermal part (dashed) and quantum mechanical part (dotted) as functions of temperature. The gray area causes the difference in fidelity between full quantum and classical data.

quantum uncertainty exceeds the effects of confinement and correlation.

To better understand the results at overlapping QD geometries, a closer inspection should be made on the origins of particle delocalization. In figure 6 the causes of total delocalization are schematically divided into thermal and quantum

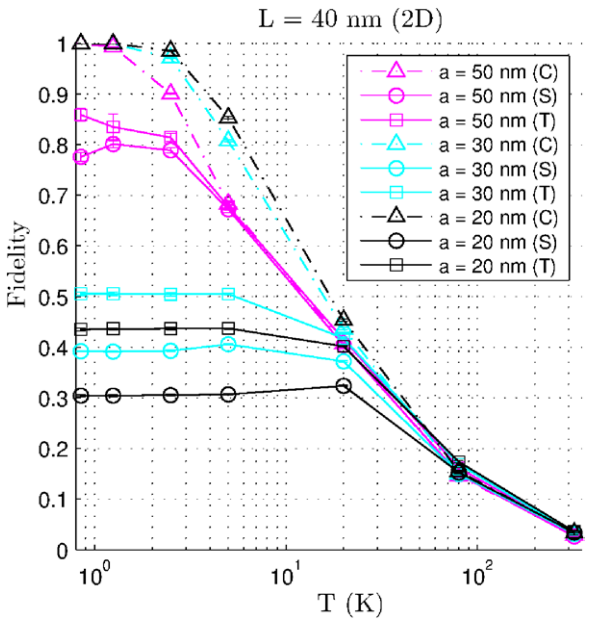

Figure 7. Comparison of computed fidelity curves for classical limit (C) and parallel (S) and antiparallel (T) spin states for 20 nm QDs in 2D.

contributions. The thermal component starts from zero and increases monotonically by temperature. The quantum component is only observed with overlapping electron densities and decays at high temperatures due to the quantum decoherence [39]. Incidentally, the minimum delocalization (maximum fidelity) is not at zero Kelvin but at some finite temperature. Conceptually, this could be exploited to achieve optimal performance, although the deviation from zero Kelvin is effectively nonexistent in any existing QCA implementation.

However, in our short separation data, this finite temperature peak in fidelity is indeed apparent, e.g. with $a = 20$ nm, $L = 40$ nm—this is the black curve in figure 5(b). The significance of the quantum delocalization is demonstrated with comparison to classical limit calculations, i.e. using Trotter number $M = 1$. These results do not exhibit the fidelity drop, hence the fidelity saturates unrestricted as the feature size decreases; this is also seen in the convergence figure 2 when $M \to 1$. The difference between classical and quantum results in figure 7 is accounted for by the quantum-originated delocalization, figure 6. Thus, a word of caution is in order: poorly justified semi-classical calculations could lead to falsely positive expectations of fidelity.

Figure 7 also includes short distance curves for triplet systems, where electron spins are parallel instead of antiparallel. The computation is carried out with RPIMC approach using free-particle nodes. Consequently, the fidelity is slightly improved, because of the repulsive exchange interaction on the same spin particles. We do not sample the simultanous ensemble of the parallel and the antiparallel spin states, but the resulting curve should lie strictly between the curves of the separate cases. Technically, parallelization of spins (for example, using a strong magnetic field) should improve the performance in delocalized regime.

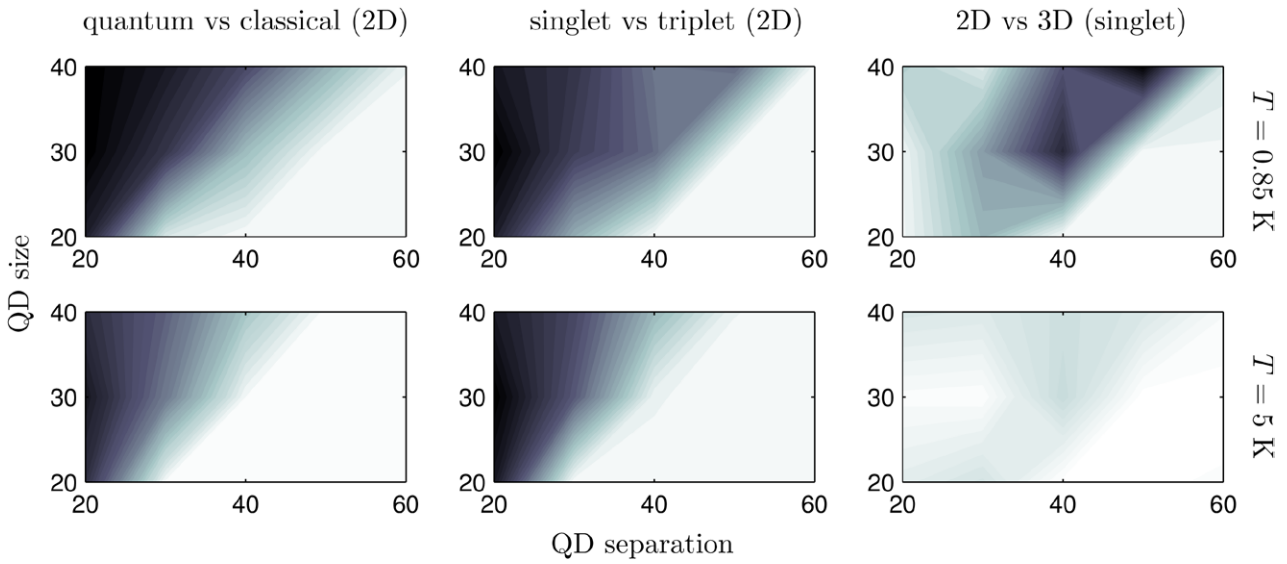

Figure 8. Comparison plots for the absolute differences between models, based on their fidelity output in L–a parameter space at temperatures of $T = 0.85$ K (top) and $T = 5$ K (bottom). From left to right: full quantum versus classical (2D), singlet spin versus triplet spin (2D) and 2D versus 3D (full quantum). Darkness describes the deviation from neutral, i.e. the importance of the appropriate choice of the model.

Finally, the thresholds for quantum phenomena are sketched on L–a-plane. The fidelity output from certain models are investigated for absolute differences $|\Delta F|$: (i) full quantum against classical in 2D, (ii) singlet spin state against triplet in full quantum 2D and (iii) 2D against 3D in full quantum. The computed differences are plotted, in respective order, in figure 8 at $T = 0.85$ K and $T = 5$ K so that the white color denotes the minimum difference in fidelity. With (i) and (ii), the relative error escalates in linear fashion the more the QDs overlap. Thus, the effects of quantum delocalization and exchange interaction should not be ignored outside the white region. Of course, the latter is only relevant, if the system is intentionally spin polarized. At higher temperatures the model may be chosen a little bit more deliberately because of the quantum decoherence. The third comparison (iii) shows that the choice of dimensionality only matters within a narrow band in the parameter space: the 3D model is not as eager to delocalize near the quantum threshold, but beyond that, yields the same results as the 2D model. However, the effects of z-dimension apart from $L_z = 5$ nm have not been properly investigated.

IV. Conclusions

Path integral Monte Carlo method was used to study the single QCA cell *fidelity*, i.e. the capability of the cell to maintain bistable polarization states in finite temperature. The system consists of two electrons in a square array of four harmonic QDs. We investigated the effects arising from temperature, singlet and triplet spin configurations, and from geometry: we varied dot–dot separation from 20 to 100 nm, and the size of the dots from 20 to 40 nm. The choice of parameters introduced two main regimes according to the localization of electronic densities. The *localized* or long range regime is essentially corresponding to the QCA paradigm. Within this region the trivial conclusion can be drawn, i.e. fidelity is decreased by increasing temperature, QD size or site separation.

However, interesting quantum effects begin to contribute at the crossover from the localized regime to the delocalized one, where the QDs start to overlap, i.e. $a \approx L$. That is, the probability density of one electron, relative to the other, is distributed into more than just one QD, causing negative impact on the fidelity. The optimization of the effects from quantum uncertainty and thermal decoherence leads to a fidelity maximum at a nonzero temperature. This is only apparent in low temperatures. Delocalization of electrons gives rise to the spin effects, which is observed as an elevated fidelity in parallel spin calculations, compared to those of antiparallel spins.

By comparison of classical and quantum simulations, we confirm the validity of 'classical limit' calculations within the localized region, only. Thus, the regime of significant QD overlap should be averted for two independent reasons: the inaccuracy of traditional QCA models, and the reduced fidelity of practical implementations. However, as is shown by the discrepancy between the delocalization of our 2D and 3D simulations, the crossover limit, or QD size, is not trivially identified even in the simplest of QD models. Moving on to more realistic potential shapes sustains the call for accurate and robust black box method, and in path integral Monte Carlo, we have just introduced one.

Acknowledgments

We acknowledge CSC—IT Center for Science Ltd. and TCSC—Tampere Center for Scientific Computing for the allocation of computational resources. We gratefully acknowledge the support of the Academy of Finland project Photonics QCA (decision number 263594).

References

[1] Tougaw P D, Lent C S and Porod W 1993 *J. Appl. Phys.* **74** 3558
[2] Tougaw P D and Lent C S 1994 *J. Appl. Phys.* **75** 1818
[3] Hänninen I and Takala J 2010 *J. Signal Process. Syst.* **58** 87–103
[4] Roohi A, DeMara R F and Khoshavi N 2015 *Microelectron. J.* **46** 531–42
[5] Momenzadeh M, Huang J, Tahoori M and Lombardi F 2005 *IEEE Trans. Comput.-Aided Des.* **24** 1881–93
[6] Tahoori M, Huang J, Momenzadeh M and Lombardi F 2004 *IEEE Trans. Nanotechnol.* **3** 432–42
[7] Gupta P, Jha N K and Lingappan L 2007 *IEEE Trans. VLSI Syst.* **15** 24–36
[8] Amlani I, Orlov A O, Snider G L, Lent C S and Bernstein G H 1998 *Appl. Phys. Lett.* **72** 2179
[9] Amlani I 1999 *Science* **284** 289–91
[10] Gardelis S, Smith C G, Cooper J, Ritchie D A, Linfield E H and Jin Y 2003 *Phys. Rev.* B **67** 033302
[11] Yadavalli K K, Orlov A O, Timler J P, Lent C S and Snider G L 2007 *Nanotechnology* **18** 375401
[12] Davies J H and Nixon J A 1989 *Phys. Rev.* B **39** 3423–6
[13] Governale M, Macucci M, Iannaccone G, Ungarelli C and Martorell J 1999 *J. Appl. Phys.* **85** 2962
[14] Lent C S and Snider G L 2014 *Lecture Notes Comput. Sci.* **8280** 3–20
[15] Wang Y and Lieberman M 2004 *IEEE Trans. Nanotechnol.* **3** 368–76
[16] Lu Y and Lent C S 2008 *Nanotechnology* **19** 155703
[17] Rahimi E and Nejad S 2012 *Nanoscale Res. Lett.* **7** 274
[18] Cowburn R P 2000 *Science* **287** 1466–8
[19] Orlov A O, Kummamuru R, Ramasubramaniam R, Lent C S, Bernstein G H and Snider G L 2003 *Surf. Sci.* **532–5** 1193–8
[20] Liu M and Lent C S 2007 *J. Electron. Test.* **23** 211–8
[21] Lent C and Tougaw P 1997 *Proc. IEEE* **85** 541–57
[22] Walus K, Dysart T, Jullien G and Budiman R 2004 *IEEE Trans. Nanotechnol.* **3** 26–31
[23] Schulhof G, Walus K and Jullien G A 2007 *ACM J. Emerging Technol. Comput.* **3** 2
[24] Yang X, Cai L, Kang Q and Zhao X 2012 *Microelectron. J.* **43** 386–92
[25] Blair E P and Lent C S 2013 *J. Appl. Phys.* **113** 124302
[26] Gin A, Tougaw P D and Williams S 1999 *J. Appl. Phys.* **85** 8281
[27] Ceperley D M 1995 *Rev. Mod. Phys.* **67** 279
[28] Harting J, Mülken O and Borrmann P 2000 *Phys. Rev.* B **62** 10207–11
[29] Leino M and Rantala T T 2004 *Phys. Scr.* **T114** 44–8
[30] Leino M and Rantala T T 2007 *Few-Body Syst.* **40** 237–52
[31] Hakkarainen T V, Luna E, Tommila J, Schramm A and Guina M 2013 *J. Appl. Phys.* **114** 174304
[32] Levinshtein M E M E, Shur M and Rumyantsev S 1996 *Handbook Series on Semiconductor Parameters* (Singapore: World Scientific)
[33] Feynman R P 1998 *Statistical Mechanics* (Reading, MA: Perseus Books)
[34] Ceperley D M 1991 *J. Stat. Phys.* **63** 1237–67
[35] Magro W R, Militzer B, Ceperley D M, Bernu B and Pierleoni C 1998 *Strongly Coupled Coulomb Systems* pp 337–40
[36] Metropolis N, Rosenbluth A W, Rosenbluth M N, Teller A H and Teller E 1953 *J. Chem. Phys.* **21** 1087
[37] Chakravarty C, Gordillo M C and Ceperley D M 1998 *J. Chem. Phys.* **109** 2123
[38] Kylänpää I, Leino M and Rantala T T 2007 *Phys. Rev.* A **76** 052508
[39] Kylänpää I and Rantala T T 2010 *J. Chem. Phys.* **133** 044312